The EMBO Journal Vol.18 No.22 pp.6271–6281, 1999

N-terminal domain swapping and metal ion binding in nitric oxide synthase dimerization

Brian R.Crane[1,2,3], Robin J.Rosenfeld[1], Andrew S.Arvai[1], Dipak K.Ghosh[4,5], Sanjay Ghosh[4], John A.Tainer[1], Dennis J.Stuehr[4] and Elizabeth D.Getzoff[1,2]

[1]Department of Molecular Biology and The Skaggs Institute for Chemical Biology, The Scripps Research Institute, La Jolla, CA 92037 and [4]Department of Immunology, The Cleveland Clinic, Cleveland, OH 44106, USA

[3]Present address: The Beckman Institute, The California Institute of Technology, Pasadena, CA 91125, USA
[5]Present address: Department of Medicine, Duke University and VA Medical Center, Durham, NC 27705, USA

[2]Corresponding authors
e-mail: crane@its.caltech.edu; edg@scripps.edu

Nitric oxide synthase oxygenase domains (NOS_{ox}) must bind tetrahydrobiopterin and dimerize to be active. New crystallographic structures of inducible NOS_{ox} reveal that conformational changes in a switch region (residues 103–111) preceding a pterin-binding segment exchange N-terminal β-hairpin hooks between subunits of the dimer. N-terminal hooks interact primarily with their own subunits in the 'unswapped' structure, and two switch region cysteines (104 and 109) from each subunit ligate a single zinc ion at the dimer interface. N-terminal hooks rearrange from intra- to intersubunit interactions in the 'swapped structure', and Cys109 forms a self-symmetric disulfide bond across the dimer interface. Subunit association and activity are adversely affected by mutations in the N-terminal hook that disrupt interactions across the dimer interface only in the swapped structure. Residue conservation and electrostatic potential at the NOS_{ox} molecular surface suggest likely interfaces outside the switch region for electron transfer from the NOS reductase domain. The correlation between three-dimensional domain swapping of the N-terminal hook and metal ion release with disulfide formation may impact inducible nitric oxide synthase (i)NOS stability and regulation *in vivo*.
Keywords: disulfide/domain swapping/β-hairpin/X-ray structure/zinc

Introduction

Nitric oxide synthases (NOSs) are highly regulated enzymes responsible for the synthesis of the potent cytotoxin and signal molecule nitric oxide (NO). NO is produced by the oxidation of L-arginine to L-citrulline via the intermediate *N*-hydroxy-L-arginine (Marletta, 1994; Griffith and Stuehr, 1995; Masters *et al*., 1996; Stuehr, 1997; Pfeiffer *et al*., 1999). NOSs are composed of two domains: (i) the catalytic oxygenase domain (NOS_{ox}) that binds heme, tetrahydrobiopterin (H_4B) and substrate L-arginine (L-arg); and (ii) the electron-supplying reductase domain (NOS_{red}) that binds NADPH, FAD and FMN. Communication between the oxygenase and reductase domains is controlled by Ca^{2+}–calmodulin, which interacts at a conserved region between NOS_{ox} and NOS_{red}, and promotes electron transfer (ET) between them.

Dimerization of the oxygenase domains is required for catalytic activity and for the binding of the essential cofactor H_4B (Marletta, 1994; Griffith and Stuehr, 1995; Masters *et al*., 1996; Stuehr, 1997; Pfeiffer *et al*., 1999). Compared with the structure of monomeric inducible (i)NOS_{ox} Δ114 (Crane *et al*., 1997), the structure of dimeric iNOS_{ox} Δ65 revealed an extensive dimer interface that creates binding sites for the two pterin molecules, sequesters the heme from solvent, and helps to structure the substrate binding site and the active-center channel (Crane *et al*., 1998). N-terminal deletion analysis and site-directed mutagenesis studies implicated an isozyme-conserved 49-residue segment in dimer formation and pterin binding (Ghosh *et al*., 1997). In the iNOS_{ox} Δ65 structure this region forms an N-terminal β-hairpin hook that connects to the subunit core near the dimer 2-fold symmetry axis. In the original structure, electron density for the connection region was difficult to discern due to high mobility and/or static disorder near the 2-fold symmetry axis, which is also crystallographic in the hexagonal space group of the iNOS_{ox} Δ65 crystals (Crane *et al*., 1998). Thus, the assignment of which N-terminal hook was associated with which subunit core was ambiguous. Based on mutagenesis data (see Ghosh *et al*., 1999) and the limited electron density in the connecting region, the N-terminal hooks were surmised to cross over and interact with adjacent subunits. Near the poorly resolved connections, Cys109 formed a self-symmetric disulfide bond with Cys109 of the adjacent subunit (Crane *et al*., 1998).

Recently, structures of dimeric rat endothelial NOS oxygenase domain (eNOS_{ox}; Raman *et al*., 1998) and human eNOS_{ox} and iNOS_{ox} (Fischmann *et al*., 1999; Li *et al*., 1999) revealed a single zinc ion ligated in the region joining the N-terminal hook to the subunit core. In these structures, the N-terminal hook regions interact primarily with their own rather than the adjacent subunits. In rat eNOS_{ox}, Cys residues 96 (murine iNOS 109) and 101 (murine iNOS 104) from both subunits provide four thiolate ligands to the zinc. Here we report that in murine, iNOS_{ox} Cys109 and previously disordered Cys104, along with the corresponding symmetry-related cysteines from the adjacent subunit, form a similar tetrahedral mononuclear metal site. This metal site orders the previously undiscernible connection and arranges the N-terminal hooks so that they interact primarily with their own subunits. However, we also report a second new iNOS_{ox} structure that better defines a zinc-free disulfide-linked

Table I. Data collection and refinement statistics for H_4B-bound dimeric $iNOS_{ox}$ with swapped and unswapped N-terminal hook regions

Structure	Swapped	Unswapped
Scatterers	7364	7202
Residues	(2 × 420)	(2 × 420)
Cofactors	2× (1Hem, 1H_4B)	2× (1Hem, 1H_4B)
Ions		1 Zn^{2+}/dimer
Disulfides	1	0
Ligands	none	2× isothiourea
Waters	396	218
Resolution	20.0–2.7 Å (2.8–2.7 Å)[a]	20.0–2.35 Å (2.43–2.35 Å)[a]
Unique reflections	39 200 (4290)[a]	62 443 (5859)[a]
Observations	153 562 (12 662)[a]	255 531 (23 654)
% completeness	91.7 (92.3)[a]	98.2 (93.9)[a]
$<I/\sigma I>$[b]	17.0 (2.9)[a]	22.6 (4.1)[a]
R_{symm}[c] (%)	5.9 (36.2)[a]	5.6 (32.1)[a]
R[d] (%)	23.6 (37.2)[a]	22.3 (40.9)[a]
Free R[e] (%)	30.6 (43.9)[a]	29.8 (43.9)[a]
<Overall B>[f] (Å^2)	59.2	47.8
<Main chain B> (Å^2)	57.7	47.2
<Side chain B> (Å^2)	60.7	49.5
R.m.s. bond[g] (Å)	0.008	0.013
R.m.s. angle[g] (°)	1.5	1.7

[a]Highest resolution bin for compiling statistics.
[b]Intensity signal to noise ratio.
[c]$R_{symm} = \Sigma\Sigma_j |I_j - <I>|/\Sigma\Sigma_j I_j$.
[d]$R = \Sigma||F_{obs}| - |F_{calc}||/\Sigma|F_{obs}|$ for all reflections (no σ cut-off).
[e]Free R calculated against 5% of the reflections removed at random. The same free reflections were chosen for both structures.
[f]Overall model average thermal (B) factor.
[g]Root mean square deviations from bond and angle restraints.

dimer. In the zinc-free structure, an alternate conformation of the metal-binding loop directs the N-terminal hooks to swap between adjacent subunits and participate extensively in the dimer interface. These results suggest roles for metal binding, disulfide formation and three-dimensional domain swapping in the regulation of NOS assembly and activity.

Results

The $iNOS_{ox}$ dimer is covalently associated either by Zn^{2+} binding or disulfide bond formation

We have determined two new crystallographic structures of dimeric murine $iNOS_{ox}$: in addition to heme and H_4B, one contains a disulfide bond across the dimer interface and has no active-center substrate or inhibitor; the other contains a tetrahedral tetrathiolate metal site in the dimer interface and the inhibitor isothiourea in the active center (Table I; Figure 1). The two structures are also distinguished by the conformation of the switch region (residues 103–111) encompassing metal-binding ligands Cys104 and Cys109 (Figures 2 and 3), and the resulting arrangement (swapped versus unswapped) of the N-terminal hooks relative to their subunit cores (Figure 1). These coupled structural differences and their consequences are the focus of this report. Otherwise, both structures match the previously published $iNOS_{ox}$ structures containing L-arg, thiocitrulline or no exogenous ligand (Crane *et al*., 1998). In our previously reported dimeric $iNOS_{ox}$ structures, Cys104 was contained in a disordered segment (residues 101–107), whereas Cys109 formed a self-symmetric disulfide bond between the subunits (Crane *et al*., 1998). Electron density for the 'swapped' structure presented here shows the same disulfide bond (Figure 2A), but also reveals defined conformations for residues 101–107 (Figure 3A). In the 'unswapped' $iNOS_{ox}$ structure, a tetrahedral metal ion is symmetrically located on the dimer 2-fold axis at the base of the two 'catcher's mitt' domain folds, 14.0 Å from each pterin ring and 21.7 Å from each heme iron (Figures 1B and 2B). The ligands Cys104 and Cys109 project from the bottom of a type I β-turn between residues 105 and 108. As with eNOS (Raman *et al*., 1998; Fischmann *et al*., 1999), the main chain nitrogen of Leu110 hydrogen bonds to the Cys 104 thiolate, whereas the main chain nitrogen of Gly111 hydrogen bonds to the Cys 109 thiolate (Figure 3B). In the absence of metal ion, two of the thiolate ligands (Cys 109 from each subunit) instead form a disulfide bond, and the metal-binding loop adopts a new conformation that exposes Cys104 to solvent (Figure 3A). This change in redox and ligation state in the metal-binding loop not only affects local structure but also correlates with three-dimensional domain swapping of the N-terminal hooks (Figure 1).

In unswapped $iNOS_{ox}$ zinc is the non-heme metal. The tetrahedral geometry and ligand complement of the metal site in unswapped $iNOS_{ox}$ suggest either a zinc or iron ion (Holm *et al*., 1996). X-ray absorption spectroscopy indicates that crystals of unswapped $iNOS_{ox}$ contain specifically bound zinc ions (data not shown), even when soaked for days in buffer containing Fe(II) and reducing agents, but no added zinc. Finally, others have shown that the metal ion bound to their NOS preparations was also zinc (Raman *et al*., 1998; Fischmann *et al*., 1999; Li *et al*., 1999). Thus, although metal ion identity *in vivo*

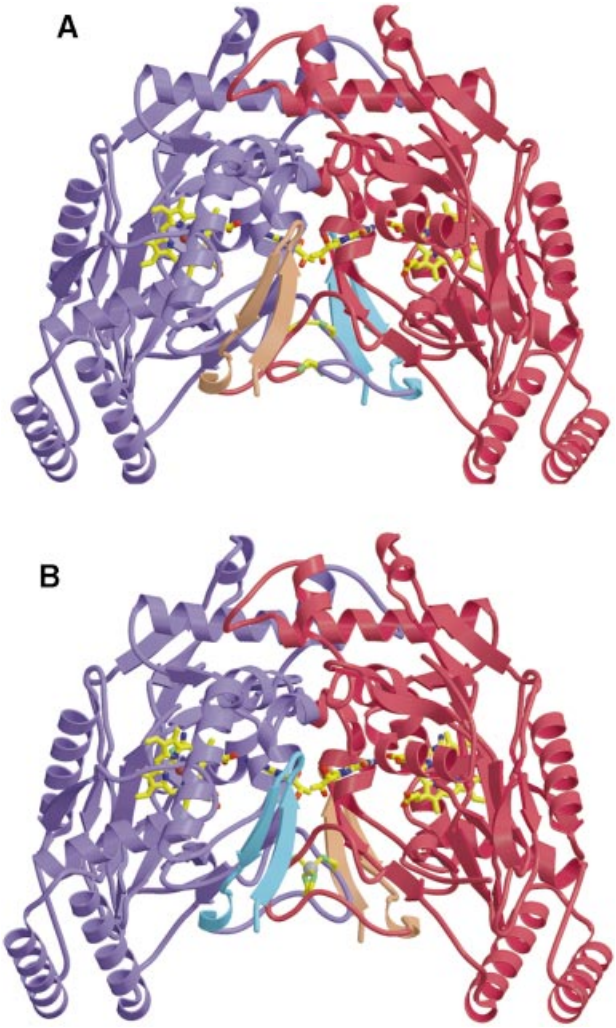

Fig. 1. The effect of domain swapping on the N-terminal hook conformation in $iNOS_{ox}$. Ribbon representation of the $iNOS_{ox}$ dimer in swapped (**A**) and unswapped (**B**) conformations. N-terminal hook regions (cyan and orange) interact primarily with their own subunits (purple and red) in the unswapped conformation, but reach across to associate with the opposite subunit in the swapped conformation. Each heme (yellow bonds) is cupped in the inward-facing palm of the central webbed β-sheet of the 'catcher's mitt' subunit fold. A self-symmetric disulfide bond (yellow, bottom center) links the two subunits in the swapped conformation (A). A single zinc ion (gray, bottom center) is bound between the two subunits at the base of the catcher's mitts in the unswapped conformation (B). Two molecules of H_4B (yellow, center, on edge) are also bound at the interface and line the active-center channels leading to the hemes.

is unknown, Zn^{2+} can occupy the tetrathiolate site in recombinant NOS_{ox}.

Interestingly, growing $iNOS_{ox}$ crystals in the presence of Fe^{2+} and ascorbate generated the swapped structure with an ordered switch region and no metal ion at the dimer interface. Thus, at least in the crystal, the $iNOS_{ox}$ tetrathiolate metal site has low affinity for Fe(II) under reducing conditions. The ability to discern electron density for the loop preceding the Cys109 disulfide (residues 101–107), which had been disordered in all previous zinc-free NOS structures (Crane *et al*., 1998; Li *et al*., 1999), may be due to the presence of ascorbate during synchrotron diffraction data collection. Disulfide bonds are electrophilic targets (Jones *et al*., 1987; Symons, 1995) for electrons ejected by synchrotron radiation, and ascorbate is known to protect proteins against ionizing radiation (Harapanhalli *et al*., 1996; Platzer and Getoff, 1998; Svoboda and Harms-Ringdahl, 1999). Radiation damage during X-ray exposure, accentuated by the proximity of the Cys109 disulfide, may hamper resolution of the exposed cysteine ligation loop in the absence of protectants.

Zinc binding is a structural switch for domain swapping of the N-terminal hook

In an example of three-dimensional domain swapping (Heringa and Taylor, 1997; Schlunegger *et al*., 1997), the two conformations of the zinc-binding loop determine which subunit core interacts primarily with which N-terminal hook (Figure 1). Characteristic of domain swapping in multimeric proteins, the N-terminal hook exchanges between identical intra- and intersubunit interfaces. Only residues 104–107 in the switch region (Figures 3 and 4) substantially change conformation on N-terminal hook swapping (Figure 2C and D). In the unswapped conformation, the type I β-turn formed by switch residues 105–108 is associated perpendicularly to its symmetry mate by zinc ion coordination of flanking residues Cys104 and Cys109 (Figure 3B). Residues 108 and 109 form main chain hydrogen bonds with residues 476 and 477 on an antiparallel strand of the adjacent subunit. In the swapped arrangement, residues 104–107 change conformation to structure the switch region as two nested β-turns (102–105 and 105–108) that share Lys105 (Figure 3A). The newly formed β-turn (102–105) fits into a pocket created by residues 105–118 of the opposing subunit. Some $iNOS_{ox}$ crystals show the presence of both switch conformations and partial occupancy for the metal ion (data not shown). A mixture of states in a single crystal suggests that both conformations can be populated in a given protein preparation.

With the exception of the switch region, the entire swapped and unswapped structures are virtually identical in residue conformation. Although the residues in the dimer interface change, most of the inter-residue contacts remain the same, including internal hydrogen bonds, salt bridges and packing interactions. Exposure of Lys117 (Ghosh *et al*., 1997), which is proteolytically sensitive in the absence of pterin, is the same regardless of zinc binding. A recent structure of zinc-free human $iNOS_{ox}$ also contained a self-symmetric disulfide bond (Li *et al*., 1999). Swapping could not be evaluated though, because the connections between the N-terminal hook and subunit core were not discerned in the electron density. The considerable disorder in the zinc-binding loop propagated to the pterin-binding segment and caused the Gly111–Ser112 (Gly117 and Ser118 for human iNOS) peptide bond to flip. The cystene-ligation site in our murine $iNOS_{ox}$ structure is well ordered and no influence of metal ion occupancy on pterin-binding residues is observed in this crystal form, including the Gly111 carbonyl flip.

Implications of swapping for dimer stability

Domain swapping results in a more extensive dimer interface for the swapped conformation than for the unswapped conformation (Figures 1 and 4). The

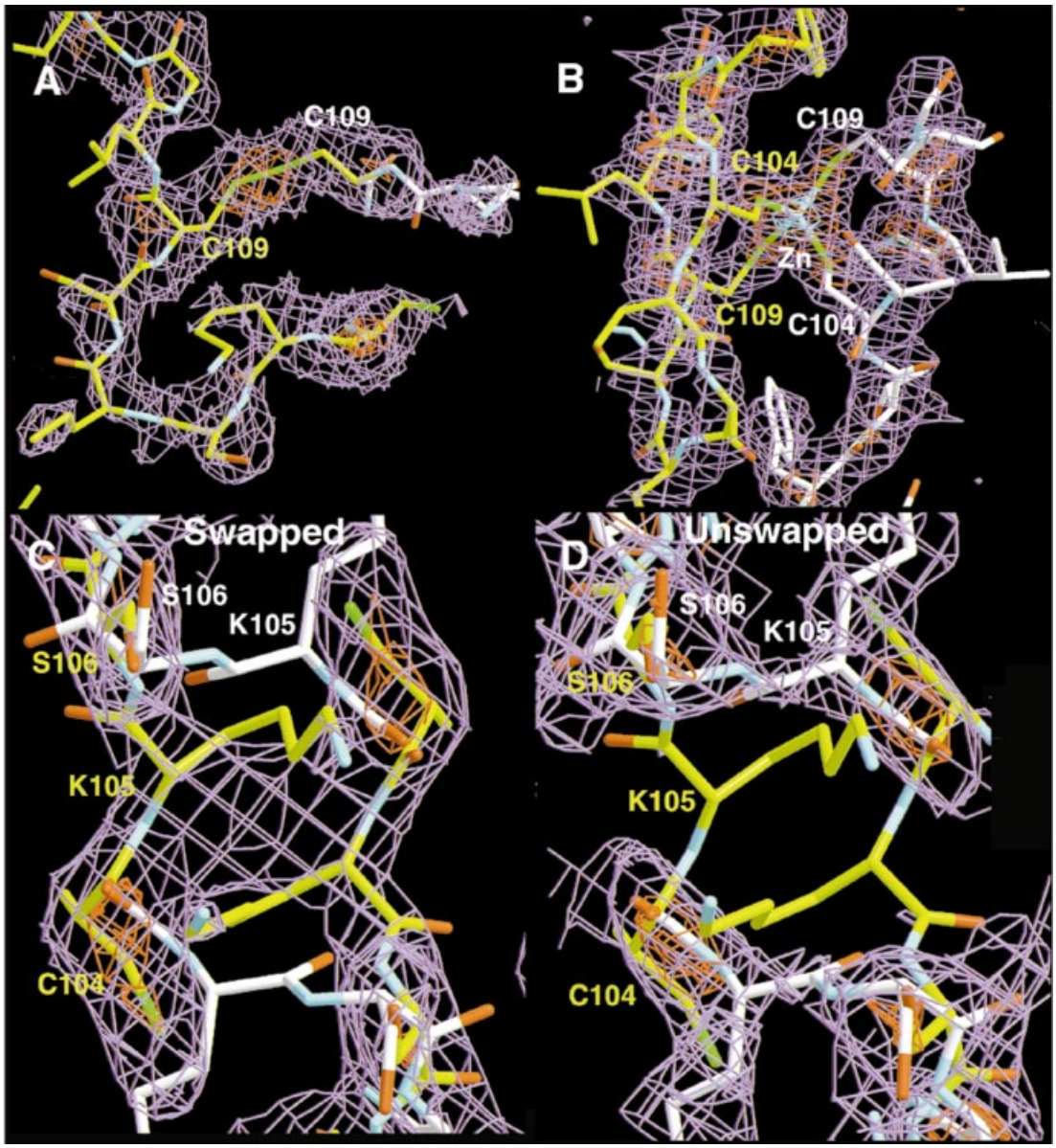

Fig. 2. Electron density at the cystene-ligation center and switch point for swapped and unswapped structures. Simulated annealed σ_A-weighted $F_{obs} - F_{calc}$ omit maps shown for the two structures (2.7 and 2.35 Å resolution for swapped and unswapped, respectively) at the disulfide/zinc center and the swapping switch point. (**A**) A disulfide bond between two symmetry-related Cys109 residues links the two subunits (yellow and white) in the swapped $iNOS_{ox}$ structure (electron density contours: purple at 2σ, red at 4σ). (**B**) The Cys109 disulfide is replaced by a tetrathiolate zinc center in unswapped $iNOS_{ox}$ (contours: purple at 3σ, red at 6σ, cyan at 11σ). (**C** and **D**) The switch point for domain swapping of the N-terminal hook. Omit electron density indicates two distinctly different conformations for residues 104–107 in the swapped [(C) 2.0σ purple contours, 4.0σ red contours] and unswapped [(D) 2.2σ purple contours, 5.0σ red contours] $iNOS_{ox}$ structures. The swapped conformation (yellow bonds) and unswapped conformation (white bonds) are shown superimposed on both electron density maps.

N-terminal hook buries approximately three times more surface area per subunit in the swapped (532.0 Å) compared with the unswapped state (184.0 Å). In both conformations, the N-terminal hook and the C-terminal end of the subunit form interactions between β1′ and residues 471–479, which include β12a, and between β2′ and residues 445–450, which include the C-terminal end of α9 (Figure 4). The side chain of Asn83 hydrogen bonds to Gln472, that of Trp84 to Glu473, and that of Asp92 to both Tyr445 and Tyr477. Interactions of the N-terminal hook with the N-terminal pterin binding segment are dominated by a packing interaction between Trp84 and Met114, and hydrogen bonds from Glu473 that bridge residues on the pterin-binding segment to β20. With the exception of the Trp84–Met114 contact, these interactions are intermolecular in the swapped conformation, whereas they occur within a subunit in the unswapped conformation.

Mutations that destabilize the iNOS dimer, reduce activity, and affect pterin and substrate binding, disrupt interactions across the dimer interface only in the swapped configuration (Table II; Ghosh *et al*., 1999). Ghosh *et al*. (1999) report two classes of mutations in the N-terminal hook region that adversely affect NOS function: (i) incorrigible mutations (N83A, D92A and H95A) whose negative effects are extreme and permanent; and (ii)

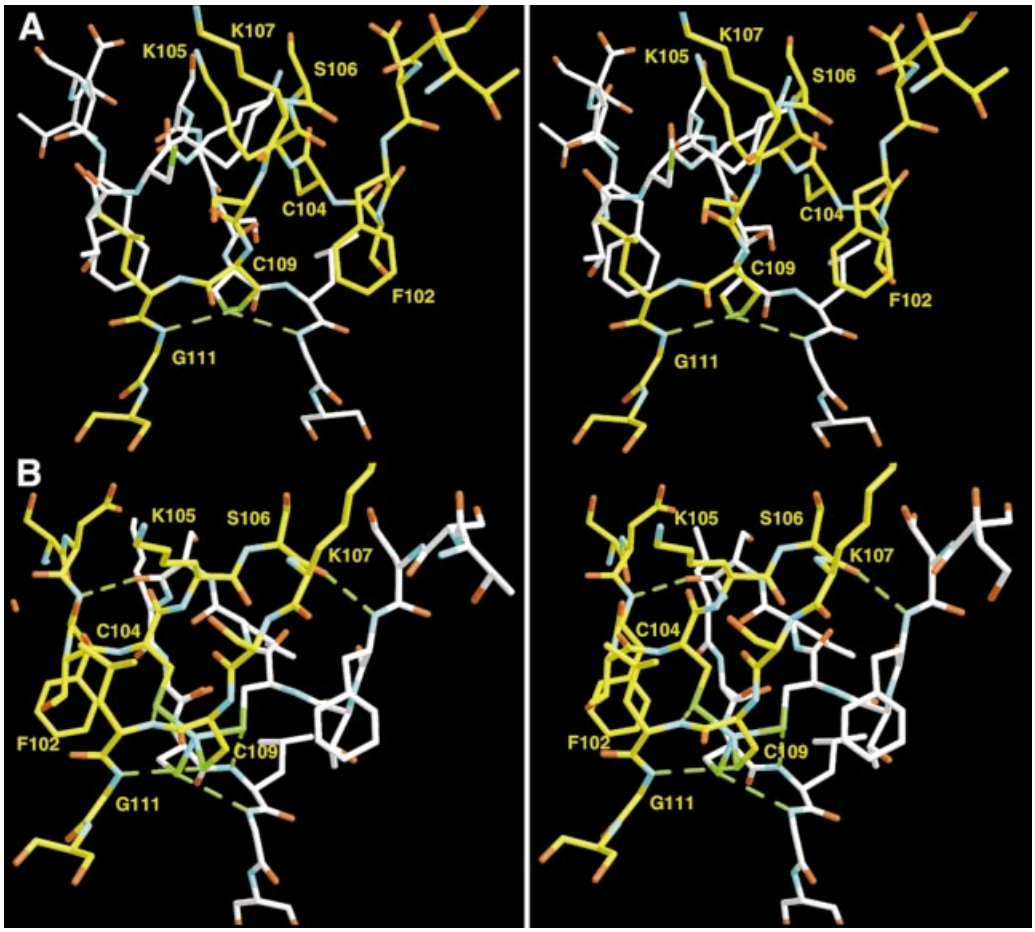

Fig. 3. Differences in the switch region upon binding zinc and swapping the N-terminal hooks. (**A**) Stereoview of the cysteine ligation loop (Figure 4) showing the disulfide bond between symmetry-related Cys109 residues that connects the two subunits of the dimer (yellow or white bonds) in the swapped structure. The Cys109 thiolate also hydrogen bonds with the Gly111 peptide nitrogen (green dashes) but the Cys104 thiolate is flipped away from the interface and exposed to solvent. (**B**) Stereoview of the same region as in (A), with Zn^{2+} (cyan, bottom center) ligated by Cys104 and Cys109 from each subunit of the unswapped dimer. Two β-turns (residues 105–108) of the two subunits stack perpendicularly at the dimer interface. A conformational change for residues 104–106 switches the connection to the N-terminal hooks relative to (A). The peptide nitrogens of Gly111 and Leu110 hydrogen bond to the thiolates of Cys109 and Cys104, respectively. There is an intersubunit hydrogen bond between the main chain atoms of Phe102 and Ser106.

reformable mutations (K82A and T93A) whose negative effects can be rescued by high levels of H_4B. Mutations of conserved N-terminal hook residues that do not make contacts with the C-terminal end of the $iNOS_{ox}$ subunit have little effect (R80A and K97A). The relatively conservative mutations of D92A and N83A are incorrigible in that they completely abolish dimerization and activity in $iNOS_{ox}$. Significantly, these residues involve interactions between β2′ and the C-terminal end of α9 that contribute to the dimer interface only in the swapped conformation. Other mutations that destabilize the $iNOS_{ox}$ dimer also involve residues that hydrogen bond and/or provide contacts across the dimer interface primarily in the swapped structure (K82A, T93A, Table II). Furthermore, mutation of Trp84, which contributes to the dimer interface in the unswapped state, has minor if any destabilizing effects on the solution dimers (Table II). Although incorrigible mutation H95A would remove similar side chain surface area in either the swapped or unswapped interfaces, it also disrupts hydrogen bonding interactions internal to the N-terminal hook and may thereby destabilize its conformation in both the swapped and unswapped states.

Implications of the zinc site for protein–protein interactions

Given their large size, there may be multiple sites of association between NOS_{ox} (~60 kDa) and NOS_{red} (~70 kDa). A precise understanding of NOS domain interactions will require analysis of a full-length NOS structure. Nevertheless, residue conservation and electrostatic potential can be useful markers for identifying surface regions of NOS_{ox} important for interactions with other domains or molecules (Honig and Nicholls, 1995; Mol *et al*., 1998). Using these criteria we have identified three positions on $iNOS_{ox}$ that may participate in protein–protein interactions. We previously suggested (Crane *et al*., 1998) that the surface on the back side of the heme could be a position for NOS_{red} interactions because of high residue conservation among NOS isozymes, exposure of the heme edge, and shape complementarity between $iNOS_{ox}$ and a model of $iNOS_{red}$ based on the structure of P-450 reductase. The surface surrounding the zinc site has also been suggested as a possible interaction region for the NOS reductase domain based on the ability of zinc sites to mediate protein–protein interactions in other

systems and the electrostatic complementarity between the eNOS and cytochrome P-450 reductase (Raman *et al*., 1998). Calculation of an electrostatic surface for $iNOS_{ox}$ with an intact zinc site reveals that the positive electrostatic potential surface previously visualized on eNOS is absent on murine $iNOS_{ox}$ (Figure 5B, Region 2). In fact, the surface surrounding the aforementioned exposed heme edge (Figure 5A, Region 1) is more positively charged than the surface surrounding the zinc. Similarly, residue conservation between isozymes is also more pronounced on the surface surrounding the exposed heme edge than on the surface surrounding the zinc site (Figure 5C and D). Thus, electrostatic potential and residue conservation at the molecular surface suggest that Region 1 is more likely than Region 2 to interact with NOS_{red}. Additionally, we note that a large pocket extending from Region 1 and

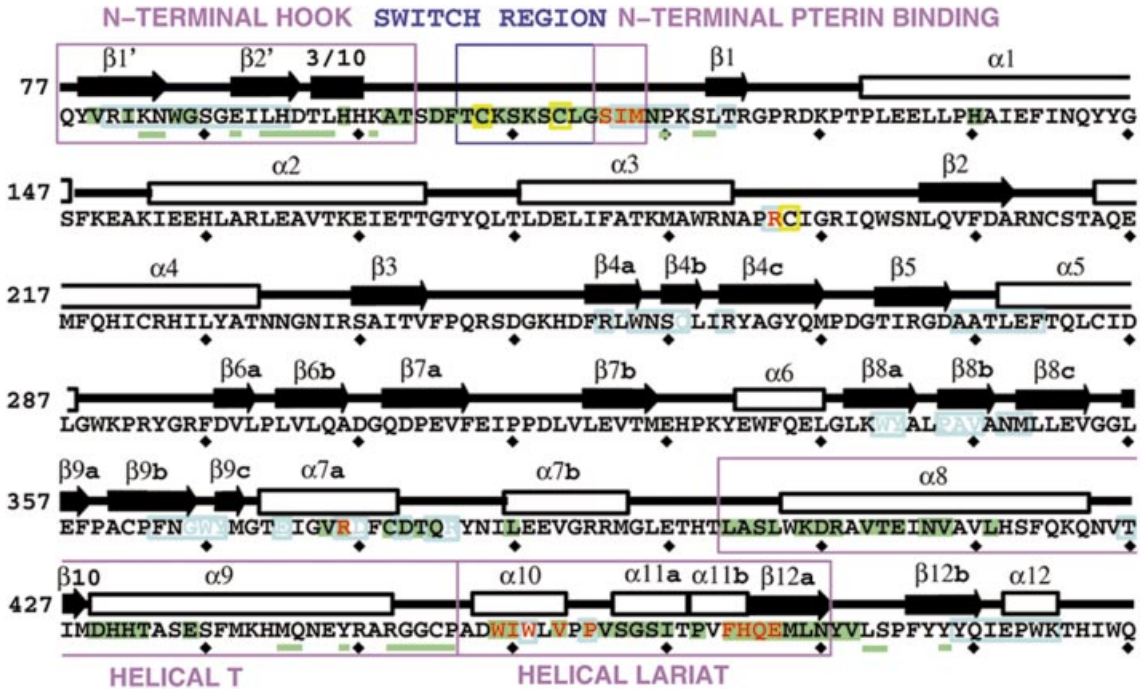

Fig. 4. Residue function, secondary structure and contributions to the dimer interface mapped onto the iNOS sequence. The murine $iNOS_{ox}$ sequence (DDBJ/EMBL/GenBank accession No. M84373) is color coded to highlight zinc ligands Cys104 and Cys109 and proximal heme ligand Cys194 (yellow boxed), L-Arg-binding residues (cyan letters), H_4B-binding residues (red letters) and residues that form the active-center channel leading to the heme (cyan boxed). Dimer interface residues that contribute at least 5 Å of buried surface area in the unswapped state are shown with green background, whereas those additional residues that contribute to the dimer interface in the swapped state are underlined in green. Above, black arrows show β-strands, white boxes show α-helices. Below, solid diamonds mark every tenth position, from 86 to 496. Key sequence stretches involved in forming the dimer interface and cofactor binding sites are outlined in large boxes and denoted N-terminal hook, switch region (zinc loop), N-terminal pterin-binding, helical T and helical lariat. Definitions of the N-terminal hook and pterin-binding segment differ slightly from Crane *et al*. (1998) due to resolution of the switch region in the new structures. Single-letter abbreviations for the amino acid residues are as follows: A, Ala; C, Cys; D, Asp; E, Glu; F, Phe; G, Gly; H, His; I, Ile; K, Lys; L, Leu; M, Met; N, Asn; P, Pro; Q, Gln; R, Arg; S, Ser; T, Thr; V, Val; W, Trp; Y, Tyr.

Table II. Structure–function relationships for N-terminal hook residues

Residue	Interactions with C-terminus		Buried surface area (Å^2)				Phenotype of Ala mutant	
	Main chain	Side chain	Main chain		Side chain		Dimerization	Dimer activity
			sw[b]	unsw[c]	sw	unsw		
R80	none	none	0.0	0.0	0.0	0.0	normal	normal
K82	N to E473 OE1 O to E473 N	none	21.3	0.0	4.8[a]	0.0	requires excess pterin	normal
N83	none	ND2 to Q472 OE1	11.0	0.0	40.1	0.0	mostly monomer	10% wild type
W84	N to H471O	NE1 to E473 OE2	7.2	9.9	25.2	58.4	normal	normal
D92	none	OD1 to Y477 OH OD2 to Y445 OH and Y447 OH	13.8	0.0	38.6	0.0	monomer	none
T93	N to G449 O	none	6.2	0.0.	9.8[a]	0.0	requires excess pterin	normal
H95	none	none	13.9	5.4	18.1	20.9	monomer	none
K97	none	none	8.1	0.0	5.7[a]	0.0	normal	normal
C109	O to N476 N	Zn ligand or disulfide	18.1	21.1	27.1	38.4	requires excess pterin	normal

[a]>80% of side chain surface area buried in the dimer interface involves C_β. Thus, these interactions are conserved on mutation to Ala.
[b]Swapped structure.
[c]Unswapped structure.

formed by α1, α3, α9 and the loop separating β12a and β12b has a high degree of positive character and conservation (Figure 5, Region 3). NOS_{red} binding at this location could place the electron-donating FMN below the proximal side of the heme and adjacent to the loop that contains the heme-ligating thiolate of Cys194.

Significantly, swapping of the N-terminal hooks and zinc binding change the molecular surface in the switch region. For example, comparing the metal-bound with the metal-free structure, Thr103 and Lys105 more than double their exposed surface area, whereas the Cys104 side chain becomes almost completely buried. Thus, interactions of NOS_{ox} with other NOS domains or different proteins near the metal site could be regulated by metal ion incorporation.

Discussion

In proteins, tetrahedral zinc ions with thiolate ligands often stabilize structure and sometimes participate in catalysis (Berg and Shi, 1996). The ligand complement for these sites (see the Metalloprotein Database and Browser, http://metallo.scripps.edu) is usually $Zn^{2+}(His)_2(Cys^-)_2$, $Zn^{2+}(His)_1(Cys^-)_3$ or $Zn^{2+}(Cys^-)_4$, with stability of the center decreasing with increasing negative charge. Thus, the net negative charge of the NOS zinc site creates the least stable of the known tetrahedral zinc centers. $Zn^{2+}(Cys^-)_4$ sites involved in stabilization of structure and interfaces are widespread in proteins that include zinc fingers (Berg and Shi, 1996; Green *et al*., 1998), cytochrome oxidase (Tsukihara *et al*., 1996), alcohol dehydrogenase (Eklund *et al*., 1976), aspartate transcarbamylase (Lipscomb, 1994) and guanine nucleotide exchange proteins (Burton *et al*., 1997). Catalytic roles of tetrathiolate-ligated zinc are known only for the Ada and related DNA repair enzymes (Demple *et al*., 1985). Ada exploits the nucleophilic properties of a displaced thiolate from the $Zn^{2+}(Cys^-)_4$ cluster to react with electrophilic moieties in alkylated DNA (Samson, 1992; Wilker and Lippard, 1995). Because the NOS zinc site is distant from the catalytic center, the zinc is unlikely to participate directly in NO synthesis, although formation of the zinc site will stabilize the unswapped dimer relative to free thiols. Protein stabilization from the zinc cluster will come not only from the covalent bonds to the zinc itself, but also from the surface area buried in the switch region. Cys104 and Cys109 must be important to NOS enzyme function given their high degree of conservation among isozymes from various species (Raman *et al*., 1998; Ghosh *et al*., 1999). However, because bound zinc has currently

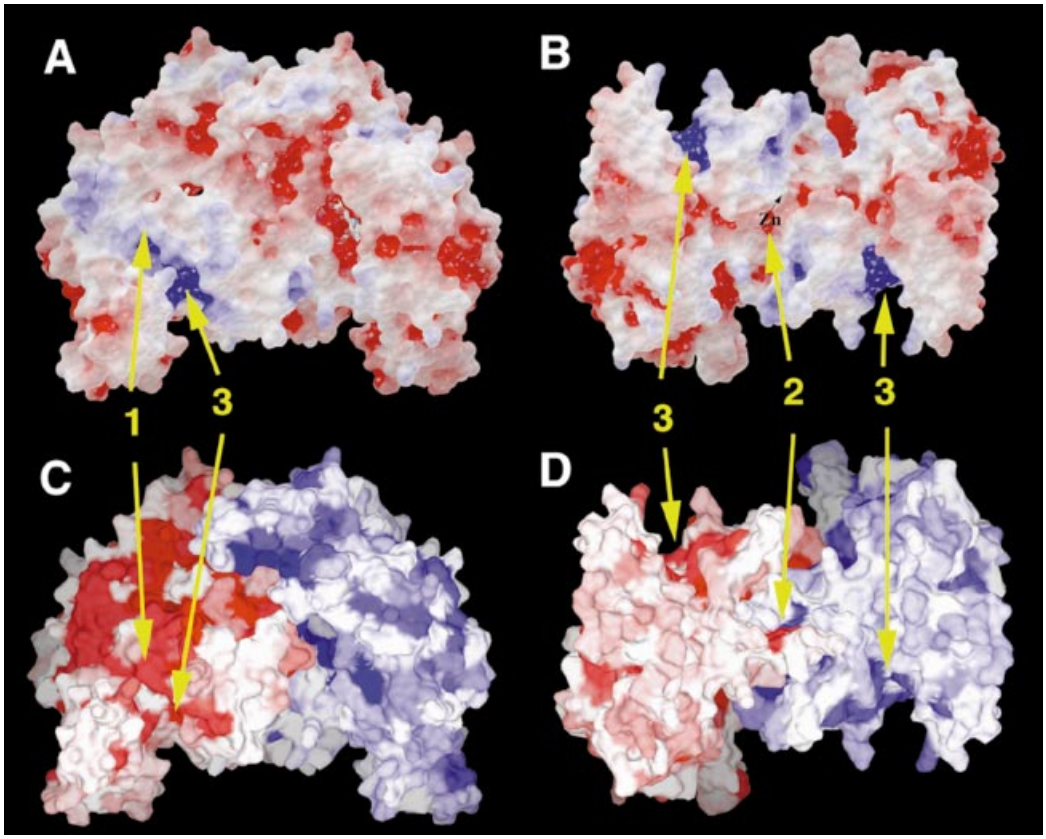

Fig. 5. Potential interaction surfaces of $iNOS_{ox}$. (**A** and **B**) Electrostatic potential mapped onto the solvent-accessible molecular surface of the unswapped zinc-bound $iNOS_{ox}$ dimer. In the left orientation (A) (matching Figure 1), surface surrounding the exposed heme edge (Region 1) is surrounded by significant positive (blue) electrostatic potential (contoured at 3 kT/q; k = Boltzmann constant, T = temperature, q = 1 point charge), whereas the region surrounding the zinc site [(B), Region 2] (right view, rotated 90° about a horizontal axis) is neutral or negative (red). A pocket adjoining Region 1 and near the heme-ligating thiolate also has significant positive potential and residue conservation (Region 3). (**C** and **D**) Solvent-accessible surface of the $iNOS_{ox}$ dimer (one subunit red, the other subunit blue) color coded by residue conservation (paler to more saturated represents less conserved to more conserved), based on a group of NOS oxygenase domain sequences representative of known species and isozymes. Conservation of surface residues is most pronounced around the exposed heme edge (Region 1) and in a region proximal to the heme thiolate (Region 3), and is low around the zinc site (Region 2).

only been characterized from NOS protein expressed in heterologous systems, alternate or additional roles for these cysteines in mammalian cells are possible. Isozymes of alcohol dehydrogenase isolated from liver can differ from each other by variable disulfide bond formation involving cysteines that can also ligate a non-catalytic zinc ion (Jörnvall, 1973; Eklund *et al*., 1976). In fact, stoichiometries of zinc content vary among different alcohol dehydrogenases, despite high conservation of ligands for both the catalytic and structural zinc sites (Clark-Baldwin *et al*., 1998). Moreover, zinc release from *Escherichia coli* threonine dehydrogenase has been correlated with cysteine oxidation to cystine (Clark-Baldwin *et al*., 1998). Recent studies on metallothionein indicate that disulfide bond formation from metal-chelating thiolates may be a general mechanism for proteins to release and transfer zinc ions in cells (Jacob *et al*., 1998; Jiang *et al*., 1998; Maret and Vallee, 1998). Interestingly, the sequence motif surrounding the NOS zinc site (TCKSKSCLG, underlined letters denote the zinc ligands) is also conserved in the extracellular domain of the insulin receptor (TCCSQDCLG, *Drosophila*), where it forms two disulfide bonds that associate perpendicular loops of polypeptide in a way that resembles the structure surrounding the NOS zinc site (Garrett *et al*., 1998). Thus, the ability of Cys109 in iNOS to form either a tetrahedral zinc site or a disulfide may have significance in mammalian cells and at the very least warrants further investigation.

A swapped configuration of the N-terminal hook is the most compelling interpretation of the mutagenesis experiments presented in Ghosh *et al*. (1999). Mutations of N-terminal hook residues that form intersubunit contacts only in the swapped conformation (Asn83, Asp92 and His95) produce the most drastic reductions in dimer stability, whereas mutations of residues that make large intersubunit contacts in the unswapped structure (Trp84) have marginal effects on dimer stability (Table II). Even mutations that are likely to act only to destabilize the N-terminal hook main chain (K82A and D93A) can still disrupt the dimer (Ghosh *et al*., 1999). Similar results (Iwasaki *et al*., 1999) have been found for the equivalent neuronal (n)NOS residues Asp314 (iNOS Asp92) and Thr315 (iNOS Thr93). Destabilization of the N-terminal hook against its own subunit could explain these mutational effects in the unswapped structure if the local structural perturbations were to propagate to regions involved in the dimer interface, such as the helical lariat or N-terminal pterin-binding segment (Figure 4). However, the extreme sensitivity of the $iNOS_{ox}$ dimer to relatively minor changes in the N-terminal hook strongly suggests that this region has a direct role in the dimer interface.

Heterodimer experiments with full-length iNOS G450A and N-terminally mutated $iNOS_{ox}$ also indicate that a functional dimer can only form when a functional N-terminal hook from one subunit interacts with a functional C-terminus of the opposite subunit (Ghosh *et al*., 1999). Two G450A full-length proteins can not dimerize and neither can two N-terminally truncated or mutated $iNOS_{ox}$ domains (e.g. Δ114, D92A, N83A). In the heterodimer, at least one of the two interfaces formed between the G450A region and the N-terminal hook must be robust for function. Furthermore, only the $iNOS_{ox}$ domain of the heterodimer is active because NOS transfers electrons from the reductase domain of one subunit to the oxygenase domain of the other (Siddhanta *et al*., 1998). The rescue of otherwise inactive N-terminally mutated $iNOS_{ox}$ domains by full-length G450A indicates that the intact N-terminus from the full-length subunit must promote a functional dimeric association by interacting with the native C-terminus of the $iNOS_{ox}$ domain. If instead the primary N-terminal hook interactions in these experiments were unswapped there would be no stable interface between full-length iNOS and its own N-terminal hook because of the G450A mutation, and no stable interface between the $iNOS_{ox}$ domain and its own N-terminal hook because of the $iNOS_{ox}$ N-terminal hook mutation. Therefore, heterodimer experiments strongly support significant N-terminal swapping in solution, and together with the structural data prompt hypotheses regarding domain swapping in the regulation of NOS assembly and activity.

Zinc-controlled domain swapping of the N-terminal hook may play an important role in iNOS stability and regulation. Absence of the metal ion results in a domain-swapped dimer with an increased dimer interface, an intersubunit disulfide link, and an altered molecular surface in the switch region. NOS is another example where metal ions may mediate switching of three-dimensional domain swapping (Schlunegger *et al*., 1997). Stability lost from removal of the zinc site may be compensated for by swapping. Domain swapping of an N-terminal segment in *Pseudomonas aeruginosa* nitrite reductase increases the stability of the dimer relative to its homologue from *Thiosphaera pantotropha*, whose N-terminus is not domain swapped (Nurizzo *et al*., 1997). Interestingly, the structure of the swapped $iNOS_{ox}$ N-terminal hook is similar to that of a C-terminal 'β-finger' in the nNOS PDZ domain that is responsible for complexing nNOS with syntrophin (Hillier *et al*., 1999). Both structural units are β-hairpins that reach over to make similar interactions with an antiparallel β-strand of another protein. Thus, swapping an N-terminal β-hairpin may be a general mechanism for mediating reversible protein–protein interactions.

N-terminal hook swapping and zinc binding are not likely to affect NOS_{ox} catalytic activity beyond influencing dimer stability and molecular surface properties surrounding the switch point. In the swapped and unswapped dimers, the vast majority of the atomic positions are identical. The only exceptions are the zinc-binding ligands and the limited switch region, which are remote from the active center. NOS has been shown to bind non-heme Fe^{2+} in a manner that enhances catalysis (Perry and Marletta, 1998). This is difficult to reconcile with existing active site structures. Iron could possibly be reconstituted in the tetrathiolate metal center, although its enhancement of activity would be more likely to reflect enhanced stability than direct participation in catalysis. We have had no success reconsituting Fe(II) into the tetrathiolate site of $iNOS_{ox}$. Changes in surface properties in the switch region may affect interactions between domains of full-length iNOS and/or interactions of NOS with other proteins. A possible role for zinc ions mediating allosteric interactions between NOS subunits is not unprecedented. For example, in aspartate transcarbamylate, a tetrahedral zinc structures the region of the

ATCase regulatory subunit that contacts the catalytic subunit (Lipscomb, 1994).

Electrostatic complementarity of NOS_{ox} with NOS_{red} and conservation of surface features among isozymes suggest that the region surrounding the exposed heme edge (Figure 5, Region 1) and/or the adjoining surface proximal to the heme (Figure 5, Region 3) are better candidates for reductase domain interactions than the region surrounding the zinc site (Figure 5, Region 2). We would expect conserved residues to be involved in the interactions between NOS domains because chimeras composed of oxygenase and reductase domains from different isozymes retain function (Ortiz de Montellano *et al*., 1998). Such sequence conservation is absent at the region surrounding the zinc site. Recently, a structure of cytochrome P-450 BM3 heme domain complexed with the FMN binding subdomain of its reductase revealed that the FMN domain interacts with the heme domain at a position proximal to the heme, near the loop containing the heme-ligating thiolate (Sevrioukova *et al*., 1999). Although the heme domains of P-450 and NOS are not homologous, the loops containing their heme ligands have similar structure (Crane *et al*., 1997) and their reductase domains are homologous. Thus, the similar relationship of Region 3 to the NOS heme compared with the relationship of the FMN domain to the BM3 heme may suggest a similar mode of reductase interaction.

The NOS tetrahedral metal center is unlikely to participate directly in electron transfer (ET) between the reductase domain and the catalytic center. Mutations of Cys104 or Cys109 in all three isozymes affect pterin or substrate binding to varying degrees, but saturating conditions of these ligands restore normal catalytic activity (and therefore ET from the reductase domain) (Chen *et al*., 1995; Ghosh *et al*., 1997; Martasek *et al*., 1998). Assuming that both catalytic centers function independently in the NOS dimer, specific ET from NOS_{red} to the adjacent NOS_{ox} subunit (Siddhanta *et al*., 1998) via a metal site symmetrically positioned relative to both NOS_{ox} active centers is very unlikely.

Facile ET from a position adjacent to the exposed heme edge or proximal thiolate ligand could be necessary at a key point in catalysis. Considering a pathways model of electronic coupling (Beratan *et al*., 1991), activationless ET from a surface near the zinc site would be ~6 orders of magnitude slower than ET from the surface surrounding the exposed heme edge. An analysis of tunneling pathways from the tetrahedral metal center to the heme reveals a number of approximately equal routes that make use of the heme carboxylates, but do not necessarily include the pterin. Even though the reorganization energy for NOS_{ox} heme reduction by NOS_{red} (likely to be >800mV; Capeillereblandin, 1995; Mines *et al*., 1996) is probably much higher than the driving force (likely to be <50 mV; Vermilion *et al*., 1981; Presta *et al*., 1998; Witteveen *et al*., 1998), the average rates (1–4 s^{-1}; Abu-Soud *et al*., 1994; Presta *et al*., 1997; Witteveen *et al*., 1998) are slow enough for ET over a considerable distance (Gray and Winkler, 1996). In the structure of P-450 BM3 oxygenase complexed with its FMN domain (Sevrioukova *et al*., 1999) 18 Å separate the FMN and heme. However, the orientation of the FMN domain relative to the heme domain in the BM3 complex (heme plus FMN domains) is incompatible with the orientation of the FMN domain relative to the FAD domain in the structure of the intact reductase (FMN plus FAD domains; Wang *et al*., 1997). Thus, the average rates of ET between reductase and oxygenase may be limited by substantial conformational changes in these systems.

In conclusion, three-dimensional domain swapping of the $iNOS_{ox}$ N-terminal hook has been defined as a biophysical phenomenon. Swapping has been characterized crystallographically and strongly implicated by both mutagenesis and heterodimer experiments. The swapping switch point occurs at the NOS_{ox} dimer interface within a site that can form a tetrahedral zinc center with two conserved cysteine residues from each subunit. Taken together, our results suggest that it is unlikely that the NOS mononuclear metal site participates directly in catalysis or ET. However, the correlation of metal ion release with swapping and the ability of Cys109 to switch between zinc coordination and intermolecular disulfide formation may have implications for the regulation of NOS via alteration of dimeric stability and molecular surface properties. Reactive oxygen species and NO produced during the oxidative burst of activated macrophages alter the cellular redox environment and react specifically with thiol-ligated metal centers (Demple, 1996; Lipinski and Drapier, 1997; Piedrafita and Liew, 1998; Wink and Mitchell, 1998). In fact, NO production has been correlated with zinc release from metalloproteins (Berendji *et al*., 1997; Kroncke and Kolb-Bachofen, 1999). Thus, disulfide formation could stabilize the iNOS dimer under conditions of oxidative stress during macrophage activation. Mammalian iNOS with substoichiometric zinc *in vivo* would support a role for domain swapping in the regulation of iNOS biological activity.

Materials and methods

Protein purification and crystallization

Murine $iNOS_{ox}$ Δ65 (residues 66–498) with a fused C-terminal His_6 tag was overexpressed in *Escherichia coli* and purified in the absence of pterin or substrate by using Ni–chelate chromatography as described previously (Ghosh *et al*., 1997). Hexagonal $iNOS_{ox}$ Δ65 crystals of space group $P6_122$ [cell dimensions 213.0 × 213.0 × 114.2 Å, two molecules/asymmetric unit, Matthews coefficient (V_m) = 4.0, solvent content = 70%] were grown overnight at 4°C by vapor diffusion from protein that had been complexed with freshly dissolved H_4B. Drops contained an equal volume mixture of 17 mg/ml $iNOS_{ox}$ Δ65 in 40 mM *N*-(2-hydroxyethyl)piperazine-*N*′-(3-propane sulfonic acid) (HEPPS) pH 7.6, 10% glycerol, 1 mM dithiothreitol and 2–4 mM H_4B, and the reservoir was comprised of 50 mM 2-(*N*-morpholino)ethanesulfonic acid (MES) pH 5.5–6.5, 50 mM β-octyl-glucoside and 18–21% Li_2SO_4 or $(NH_4)_2SO_4$. Crystals were grown in the presence of 4 mM *S*-ethyl-thiourea, or 4 mM $Fe(II)Cl_2$ and 4 mM L-ascorbate for determination of the 'unswapped' and 'swapped' structures, respectively (Table I).

X-ray absorption spectroscopy

X-ray absorption spectra were recorded on single $iNOS_{ox}$ crystals at the Advanced Light Source in the Lawrence Berkeley Laboratory.

Structure determination and refinement

The crystals for both structures that were derived were isomorphous with previously determined $iNOS_{ox}$ structures. Diffraction data were collected with synchrotron radiation from the Stanford Synchrotron Radiation Laboratory at 100 K. The data sets were reduced with DENZO (Otwinowski, 1993) and scaled with SCALEPACK (Otwinowski, 1993). XFIT (McRee, 1992, 1999) was used for model building and structural analysis, while all refinement of crystallographic models was carried out with X-PLOR (Brünger *et al*., 1987). For the structure determination, a

previously refined model of $iNOS_{ox}$ Δ65 to 2.6 Å resolution (Crane *et al*., 1998), with pterin, ligands and water molecule cofactors removed, was used for initial bulk solvent and overall anisotropic temperature factor corrections. The structures were then refined by positional refinement in X-PLOR against the new diffraction data, first to 3.2 Å and then to 2.6 Å. In all data sets the same 5% of the reflections were set aside for R_{free} calculation. The loops and areas surrounding the zinc site were rebuilt to $F_{obs} - F_{calc}$ omit electron density maps, whereas the rest of the molecule, which changed little in conformation, was surveyed and adjusted with standard $F_{obs} - F_{calc}$ and $2F_{obs} - F_{calc}$ maps. Ligands were modeled into the resulting difference peaks on the distal side of the heme, and water molecules were added gradually over cycles of positional conjugate gradient refinement followed by *B*-factor refinement. Non-crystallographic symmetry restraints were maintained on 70% of the backbone atoms in the two non-identical subunits. Water molecules were placed only in difference peaks $>3\sigma$ that were 2.2–3.5 Å from appropriate protein hydrogen bonding partners. Simulated annealing omit maps calculated at the switch position for both the zinc-bound and disulfide-linked structures confirmed the swapping of the N-terminal hooks. In addition, $F_o - F_c$ difference maps calculated from each data set refined against both models, either swapped or unswapped, indicated conformational change at the switch point in the two crystals.

Electrostatic potential calculations

Electrostatic potentials were calculated with the Poisson–Boltzmann equation as implemented in Delphi (Gilson *et al*., 1985) (internal dielectric constant = 4.0, external dielectric = 80.0, ionic strength = 0.15 M, grid space = 1.4 Å). Partial charges were defined for the protein atoms by AMBER (Weiner and Kollman, 1981) and for the metal site by density functional methods (Mouesca *et al*., 1994). To avoid discontinuities at the protein–solvent boundary the potential was sampled 2.8 Å (twice the grid spacing) from the solvent-accessible surface [calculated with MS (Connolly, 1983), 1.4 Å probe radius] and then mapped back onto the surface.

Analysis of surface properties

Molecular surfaces were calculated with MS (Connolly, 1983) using a 1.4 Å probe radius. Residue conservation among NOS isozymes from known representative sequences was fit to a continuous function, mapped onto the solvent-accessible molecular surface of $iNOS_{ox}$ and expressed as degree of color saturation (Mol *et al*., 1998).

Acknowledgements

We thank the Advanced Light Source (ALS) and the Stanford Synchrotron Radiation Laboratory (SSRL) for use of data collection facilities, L.Noodleman for help with DFT calculations, A.M.Bilwes for helpful discussions, and S.J.Lloyd for excellent technical assistance. Supported by National Institutes of Health grants HL58883 (E.D.G.) and CA53914 (D.J.S.), fellowship grants from the Helen Hay Whitney Foundation (B.R.C.), La Jolla Interfaces in Science (R.J.R.) and the Skaggs Institute for Research (A.S.A. and B.R.C.).

References

Abu-Soud,H.M., Feldman,P.L., Clark,P. and Stuehr,D.J. (1994) Electron transfer in the nitric oxide synthases. *J. Biol. Chem.*, **269**, 32318–32326.

Beratan,D., Betts,J. and Onuchic,J. (1991) Protein electron-transfer rates set by the bridging secondary and tertiary structure. *Science*, **252**, 1285–1288.

Berendji,D., Kolb-Bachofen,V., Meyer,K., Grapenthin,O., Weber,H., Wahn,V. and Kroncke,K. (1997) Nitric oxide mediates intracytoplasmic and intranuclear zinc release. *FEBS Lett*., **405**, 37–41.

Berg,J. and Shi,Y. (1996) The galvanization of biology: a growing appreciation for the roles of zinc. *Science*, **271**, 1081–1085.

Brünger,A.T., Kuriyan,J. and Karplus,M. (1987) Crystallographic *R* factor refinement by molecular dynamics. *Science*, **235**, 458–460.

Burton,J., Slepnev,V. and DeCamilli,P. (1997) An evolutionarily conserved domain in a subfamily of rabs is crucial for the interaction with the guanyl nucleotide exchange factor mss4. *J. Biol. Chem.*, **272**, 3663–3668.

Capeillereblandin,C. (1995) Flavocytochrome-*b* (2) cytochrome *c* interactions—the electron-transfer reaction revisited. *Biochemie*, **77**, 516–530.

Chen,P., Tsai,A. and Wu,K. (1995) Cysteine-99 of endothelial nitric-oxide synthase (NOS-III) is critical for tetrahydrobiopterin-dependent NOS-III stability and activity. *Biochem. Biophys. Res. Commun.*, **215**, 1119–1129.

Clark-Baldwin,K., Johnson,A., Chen,Y., Dekker,E. and Penner-Hahn,J. (1998) Structural characterization of the zinc site in *Escherichia coli* L-threonine dehydrogenase using extended X-ray absorption fine structure spectroscopy. *Inorg. Chim. Acta*, **276**, 215–221.

Connolly,M.L. (1983) Solvent-accessible surfaces of proteins and nucleic acids. *Science*, **221**, 709–713.

Crane,B.R., Arvai,A.S., Gachhui,R., Wu,C., Ghosh,D.K., Getzoff,E.D., Stuehr,D.J. and Tainer,J.A. (1997) The structure of nitric oxide synthase oxygenase domain and inhibitor complexes. *Science*, **278**, 425–431.

Crane,B.R., Arvai,A.S., Ghosh,D.K., Wu,C., Getzoff,E.D., Stuehr,D.J. and Tainer,J.A. (1998) Structure of nitric oxide synthase oxygenase dimer with pterin and substrate. *Science*, **279**, 2121–2126.

Demple,B. (1996) Redox signaling and gene control in the *Escherichia coli* soxRS oxidative stress regulon—a review. *Gene*, **179**, 53–57.

Demple,B., Sedgwick,B., Robins,P., Totty,N., Waterfield,M. and Lindahl,T. (1985) Active-site and complete sequence of the suicidal methyltransferase that counters alkylation mutagenesis. *Proc. Natl Acad. Sci. USA*, **82**, 2688–2692.

Eklund,H. *et al*. (1976) Three-dimensional structure of horse liver alcohol dehyrogenase at 2.4 Å resolution. *J. Mol. Biol.*, **102**, 27–59.

Fischmann,T. *et al*. (1999) Structural characterization of nitric oxide synthase isoforms reveals striking active-site conservation. *Nature Struct. Biol.*, **6**, 233–242.

Garrett,T., McKern,N., Lou,M., Frenkel,M., Bentley,J., Lovrecz,G., Elleman,T., Cosgrove,L. and Ward,C. (1998) Crystal structure of the first three domains of the type-1 insulin-like growth factor receptor. *Nature*, **394**, 395–399.

Ghosh,D.K., Wu,C., Pitters,E., Moloney,M., Werner,E.R., Mayer,B. and Stuehr,D.J. (1997) Characterization of the inducible nitric oxide synthase oxygenase domain identifies a 49 amino acid segment required for subunit dimerization and tetrahydrobiopterin interaction. *Biochemistry*, **36**, 10609–10619.

Ghosh,D.K. *et al*. (1999) Inducible nitric oxide synthase: role of the N-terminal β-hairpin hook and pterin-binding segment in dimerization and tetrahydrobiopterin interaction. *EMBO J.*, **18**, 6260–6270.

Gilson,M.K., Rashin,A., Fine,R. and Honig,B. (1985) On the calculation of electrostatic interactions in proteins. *J. Mol. Biol.*, **183**, 503–516.

Gray,H.B. and Winkler,J.R. (1996) Electron transfer in proteins. *Annu. Rev. Biochem.*, **65**, 537–561.

Green,A., Parker,M., Conte,D. and Sarkar,B. (1998) Zinc finger proteins: a bridge between transition metals and gene regulation. *J. Trace Elem. Exp. Med.*, **11**, 103–118.

Griffith,O.W. and Stuehr,D.J. (1995) Nitric oxide synthases: properties and catalytic mechanism. *Annu. Rev. Physiol.*, **57**, 707–736.

Harapanhalli,R., Yaghmai,V., Giuliani,D., Howell,R. and Rao,D. (1996) Antioxidant effects of vitamin c in mice following X-irradiation. *Res. Commun. Mol. Pathol. Pharmacol.*, **94**, 271–287.

Heringa,J. and Taylor,W. (1997) Three-dimensional domain duplication, swapping and stealing. *Curr. Opin. Struct. Biol.*, **7**, 416–421.

Hillier,B., Christopherson,K., Prehods,K., Bredt,D. and Lim,W. (1999) Unexpected modes of PDZ domain scaffolding revealed by structure of nNOS–syntrophin complex. *Science*, **284**, 812–815.

Holm,R., Kennepohl,P. and Solomon,E.I. (1996) Structural and functional aspects of metal sites in biology. *Chem. Rev.*, **96**, 2239–2314.

Honig,B. and Nicholls,A. (1995) Classical electrostatics in biology and chemistry. *Science*, **268**, 1144–1149.

Iwasaki,T., Hori,H., Hayashi,Y. and Nishino,T. (1999) Modulation of the remote heme site geometry of recombinant neuronal nitric-oxide synthase by the N-terminal hook region. *J. Biol. Chem.*, **274**, 7705–7713.

Jacob,C., Maret,W. and Vallee,B. (1998) Control of zinc transfer between thionein, metallothionein and zinc proteins. *Proc. Natl Acad. Sci. USA*, **95**, 3489–3494.

Jiang,L., Maret,W. and Vallee,B. (1998) The glutathione redox couple modulates zinc transfer from metallothionein to zinc-depleted sorbitol dehydrogenase. *Proc. Natl Acad. Sci. USA*, **95**, 3483–3488.

Jones,G., Les,J., Symons,M. and Taiwo,F. (1987) Electron spin resonance studies of radiation damage to DNA and to proteins. *Nature*, **330**, 727–773.

Jörnvall,H. (1973) Differences in thiol groups and multiple forms of rat liver alcohol dehydrogenase. *Biochem. Biophys. Res. Commun.*, **53**, 1096–1101.

Kroncke,K. and Kolb-Bachofen,V. (1999) Measurement of nitric oxide-

mediated effects on zinc homeostasis and zinc finger transcription factors. *Methods Enzymol.*, **301**, 126–135.
Li,H., Raman,C., Glaser,C., Blasko,E., Young,T., Parkinson,J., Whitlow,M. and Poulos,T. (1999) Crystal structure of zinc-free and -bound heme domain of human inducible nitric-oxide synthase. *J. Biol. Chem.*, **30**, 21276–21284.
Lipinski,P. and Drapier,J. (1997) Interplay between ferritin metabolism, reactive oxygen species and nitric oxide. *J. Biol. Inorg. Chem.*, **2**, 559–566.
Lipscomb,W. (1994) Aspartate-transcarbamylase from *Escherichia coli*—activity and regulation. *Adv. Enzymol. Mol. Biol.*, **68**, 67–151.
Maret,W. and Vallee,B. (1998) Thiolate ligands in metallothionein confer redox activity on zinc clusters. *Proc. Natl Acad. Sci. USA*, **95**, 3478–3482.
Marletta,M. (1994) Nitric oxide synthase: aspects concerning structure and catalysis. *Cell*, **78**, 927–930.
Martasek,P. *et al*. (1998) The C331A mutant of neuronal nitric-oxide synthase is defective in arginine binding. *J. Biol. Chem.*, **273**, 34799–34805.
Masters,B.S.S., McMillan,K., Sheta,E.A., Nishimura,J.S., Roman,L.J. and Martasek,P. (1996) Neuronal nitric oxide synthase, a modular enzyme formed by convergent evolution: structure studies of a cysteine thiolate-liganded heme protein that hydroxylates L-arginine to produce NO as a cellular signal. *FASEB J.*, **10**, 552–558.
McRee,D.E. (1992) A visual protein crystallographic software system for X11/Xview. *J. Mol. Graph.*, **10**, 44–46.
McRee,D.E. (1999) XtalView/Xfit—A versatile program manipulating atomic coordinates and electron density. *J. Struct. Biol.*, **125**, 156–165.
Mines,G.A., Bjerrum,M.J., Hill,M.G., Casimiro,D.R., Chang,I., Winkler,J.R. and Gray,H.B. (1996) Rates of heme oxidation and reduction in Ru (His33)cytochrome *c* at very high driving forces. *J. Am. Chem. Soc.*, **118**, 1961–1965.
Mol,C., Parikh,S. and Tainer,J. (1998) *Structural Phylogenetics of DNA Base Excision Repair.* Springer, Berlin, Germany, Vol. 12, pp. 283–438.
Mouesca,J., Chen,J., Noodleman,L., Bashford,D. and Case,D. (1994) Density-functional Poisson–Boltzmann calculations of redox potentials for iron-sulfur clusters. *J. Am. Chem. Soc.*, **116**, 11898–11914.
Nurizzo,D. *et al*. (1997) N-terminal arm exchange is observed in the 2.15 Å crystal structure of oxidized nitrite reductase from *Pseudomonas aeruginosa*. *Structure*, **5**, 1157–1171.
Ortiz de Montellano,P., Nishida,C., Rodriguez-Crespo,I. and Gerber,N. (1998) Nitric oxide synthase structure and electron transfer. *Drug Metab. Disp.*, **26**, 1185–1189.
Otwinowski,Z. (1993) In Sawyer,L., Isaacs,N. and Bailey,S. (eds), *Data Collection and Processing*. Science and Engineering Research Council, Warrington, UK, pp. 56–62.
Perry,J. and Marletta,M. (1998) Effects of transition metals on nitric oxide synthase catalysis. *Proc. Natl Acad. Sci. USA*, **95**, 11101–11106.
Pfeiffer,S., Mayer,B. and Hemmens,B. (1999) Nitric oxide: chemical puzzles posed by a biological messenger. *Angew. Chem. Int. Ed. Engl.*, **38**, 1715–1731.
Piedrafita,D. and Liew,F. (1998) Nitric oxide: a protective or pathogenic molecule? *Rev. Med. Microbiol.*, **9**, 179–189.
Platzer,I. and Getoff,N. (1998) Vitamin C acts as radiation-protecting agent. *Radiat. Phys. Chem.*, **51**, 73–76.
Presta,A., Siddhanta,U., Wu,C., Sennequier,N., Huang,L., Abu-Soud,H.M., Erzurum,S. and Stuehr,D.J. (1997) Comparative functioning of dihydro- and tetrahydropterins in supporting electron transfer, catalysis and subunit dimerization in inducible nitric oxide synthase. *Biochemistry*, **37**, 298–310.
Presta,A., Weber-Main,A., Stankovich,M. and Stuehr,D. (1998) Comparative effects of substrates and pterin cofactor on the heme midpoint potential in inducible and neuronal nitric oxide synthases. *J. Am. Chem. Soc.*, **120**, 9460–9465.
Raman,C., Li,H., Martasek,P., Kral,V., Masters,B.S. and Poulos,T.L. (1998) Crystal structure of constitutive endothelial nitric oxide synthase: a paradigm for pterin function involving a novel metal center. *Cell*, **95**, 939–950.
Samson,L. (1992) The suicidal DNA-repair methyltransferases of microbes. *Mol. Microbiol.*, **6**, 825–831.
Schlunegger,M., Bennett,M.J. and Eisenberg,D. (1997) Oligomer formation by 3D domain swapping: a model for protein assembly and misassembly. *Adv. Protein Chem.*, **50**, 61–122.
Sevrioukova,I., Li,H., Zhang,H., Peterson,J. and Poulos,T. (1999) Structure of a cytochrome p450-redox partner electron-transfer complex. *Proc. Natl Acad. Sci. USA*, **96**, 1863–1868.
Siddhanta,U., Presta,A., Fan,B., Wolan,D., Rousseau,D. and Stuehr,D. (1998) Domain swapping in inducible nitric-oxide synthase: electron transfer occurs between flavin and heme groups located on adjacent subunits in the dimer. *J. Biol. Chem.*, **273**, 18950–18958.
Stuehr,D. (1997) Structure–function aspects in the nitric oxide synthases. *Annu. Rev. Pharmacol. Toxicol.*, **18**, 707–736.
Svoboda,P. and Harms-Ringdahl,M. (1999) Protection or sensitization by thiols or ascorbate in irradiated solutions of DNA or deoxyguanosine. *Radiat. Res.*, **151**, 605–616.
Symons,M. (1995) Electron spin resonance studies of radiation damage to DNA and to proteins. *Radiat. Phys. Chem.*, **45**, 837–845.
Tsukihara,T., Aoyama,H., Yamashita,E., Tomizaki,T., Yamaguchi,H., ShinzawaItoh,K., Nakashima,R., Yaono,R. and Yoshikawa,S. (1996) The whole structure of the 13-subunit oxidized cytochrome *c* oxidase at 2.8 Å. *Science*, **272**, 1136–1144.
Vermilion,J., Ballou,D., Massey,V. and Coon,M. (1981) Separate roles for FMN and FAD in catalysis by liver microsomal NADPH-cytochrome P-450 reductase. *J. Biol. Chem.*, **256**, 266–277.
Wang,M., Roberts,D.L., Paschke,R., Shea,T.M., Masters,B.S.S. and Kim,J.J. (1997) Three-dimensional structure of NADPH-cytochrome P450 reductase: prototype for FMN- and FAD-containing enzymes. *Proc. Natl Acad. Sci. USA*, **94**, 8411–8416.
Weiner,P.K. and Kollman,P.A. (1981) AMBER: assisted model building with energy refinement. A general program for modeling molecules and their interactions. *J. Comput. Chem.*, **2**, 287–303.
Wilker,J. and Lippard,S. (1995) Modeling the DNA methylphosphotriester repair site in *Escherichia coli* ada: why zinc and 4 cysteines. *J. Am. Chem. Soc.*, **117**, 8682–8683.
Wink,D. and Mitchell,J. (1998) Chemical biology of nitric oxide: insights into regulatory, cytotoxic and cytoprotective mechanisms of nitric oxide. *Free Radic. Biol. Med.*, **25**, 434–456.
Witteveen,C., Giovanelli,J., Yim,M., Gachhui,R., Stuehr,D. and Kaufman,S. (1998) Reactivity of the flavin semiquinone of nitric oxide synthase in the oxygenation of arginine to N-G-hydroxyarginine, the first step of nitric oxide synthesis. *Biochem. Biophys. Res. Commun.*, **250**, 36–42.

Received August 18, 1999; revised and accepted September 30, 1999